

Fast-Hadamard Transforms for Compressive Sensing of Joint-Systems: Measurement of a 16.8 Million-Dimensional Entangled Probability Distribution

Daniel J. Lum^{1,2,*}, Samuel H. Knarr^{1,2}, and John C. Howell^{1,2}

¹*Department of Physics and Astronomy, University of Rochester, Rochester, New York 14627, USA*

²*Center for Coherence and Quantum Optics, University of Rochester, Rochester, New York 14627, USA*

*[*daniel.lum@pas.rochester.edu](mailto:daniel.lum@pas.rochester.edu)*

Abstract: We demonstrate how to implement extremely high-dimensional compressive imaging on a bi-photon probability distribution. When computationally reconstructing the two-party system, compressive imaging requires a sensing matrix that may drastically exceed practical limits for conventional computers. These limitations are virtually eliminated via fast-Hadamard transform Kronecker-based compressive sensing. We list, in detail, the operations necessary to implement this method and provide an experimental demonstration in which we measure and reconstruct a 16.8 million-dimensional bi-photon probability distribution. Instead of requiring over a year to raster scan or over 2 terabytes of computer memory to perform a reconstruction, we performed the experiment in approximately twenty hours, required between 8 and 32 gigabytes of computer memory, and reconstructed the full distribution in approximately twenty minutes.

© 2022 Optical Society of America

OCIS codes: (100.3010) Image reconstruction techniques, (270.0270) Quantum optics, (110.1758) Computational imaging

References and links

1. G. Masada, K. Miyata, A. Politi, T. Hashimoto, J. L. O'Brien, and A. Furusawa, "Continuous-variable entanglement on a chip," *Nature Photonics* (2015).
2. J. L. O'Brien, A. Furusawa, and J. Vučković, "Photonic quantum technologies," *Nature Photonics* **3**, 687–695 (2009).
3. F. Grosshans, A. Acín, and N. Cerf, "Continuous variable quantum key distribution," *Quantum information with Continuous Variables of Atoms and Light* pp. 63–83 (2007).
4. A. Steane, "Quantum computing," *Reports on Progress in Physics* **61**, 117 (1998).
5. S. D. Huver, C. F. Wildfeuer, and J. P. Dowling, "Entangled fock states for robust quantum optical metrology, imaging, and sensing," *Physical Review A* **78**, 063828 (2008).
6. V. Giovannetti, S. Lloyd, and L. Maccone, "Advances in quantum metrology," *Nature Photonics* **5**, 222–229 (2011).
7. M. H. Rubin, "Transverse correlation in optical spontaneous parametric down-conversion," *Physical Review A* **54**, 5349 (1996).
8. J. C. Howell, R. S. Bennink, S. J. Bentley, and R. Boyd, "Realization of the einstein-podolsky-rosen paradox using momentum-and position-entangled photons from spontaneous parametric down conversion," *Physical review letters* **92**, 210403 (2004).

9. T. E. Keller and M. H. Rubin, "Theory of two-photon entanglement for spontaneous parametric down-conversion driven by a narrow pump pulse," *Physical Review A* **56**, 1534 (1997).
 10. J. Schneeloch and J. C. Howell, "Introduction to the transverse spatial correlations in spontaneous parametric down-conversion through the biphoton birth zone," arXiv preprint arXiv:1502.06996 (2015).
 11. J. Schneeloch, P. B. Dixon, G. A. Howland, C. J. Broadbent, and J. C. Howell, "Violation of continuous-variable einstein-podolsky-rosen steering with discrete measurements," *Physical review letters* **110**, 130407 (2013).
 12. J. Schneeloch, S. H. Knarr, G. A. Howland, and J. C. Howell, "Demonstrating continuous variable epr steering in spite of finite experimental capabilities using fano steering bounds," arXiv preprint arXiv:1410.8853 (2014).
 13. A. I. Lvovsky and M. G. Raymer, "Continuous-variable optical quantum-state tomography," *Reviews of Modern Physics* **81**, 299 (2009).
 14. D. Giovannini, J. Romero, J. Leach, A. Dudley, A. Forbes, and M. J. Padgett, "Characterization of high-dimensional entangled systems via mutually unbiased measurements," *Physical review letters* **110**, 143601 (2013).
 15. M. P. Edgar, D. S. Tasca, F. Izdebski, R. E. Warburton, J. Leach, M. Agnew, G. S. Buller, R. W. Boyd, and M. J. Padgett, "Imaging high-dimensional spatial entanglement with a camera," *Nature communications* **3**, 984 (2012).
 16. R. Fickler, M. Krenn, R. Lapkiewicz, S. Ramelow, and A. Zeilinger, "Real-time imaging of quantum entanglement," *Scientific reports* **3** (2013).
 17. G. A. Howland and J. C. Howell, "Efficient high-dimensional entanglement imaging with a compressive-sensing double-pixel camera," *Physical Review X* **3**, 011013 (2013).
 18. P. B. Dixon, G. A. Howland, J. Schneeloch, and J. C. Howell, "Quantum mutual information capacity for high-dimensional entangled states," *Physical review letters* **108**, 143603 (2012).
 19. D. L. Donoho, "Compressed sensing," *Information Theory, IEEE Transactions on* **52**, 1289–1306 (2006).
 20. M. F. Duarte, M. A. Davenport, D. Takhar, J. N. Laska, T. Sun, K. E. Kelly, and R. G. Baraniuk, "Single-pixel imaging via compressive sampling," *IEEE Signal Processing Magazine* **25**, 83 (2008).
 21. F. Tonolini, S. Chan, M. Agnew, A. Lindsay, and J. Leach, "Reconstructing high-dimensional two-photon entangled states via compressive sensing," *Scientific reports* **4** (2014).
 22. Y. Rivenson and A. Stern, "Practical compressive sensing of large images," in "Digital Signal Processing, 2009 16th International Conference on," (IEEE, 2009), pp. 1–8.
 23. M. F. Duarte and R. G. Baraniuk, "Kronecker compressive sensing," *Image Processing, IEEE Transactions on* **21**, 494–504 (2012).
 24. I. W. Selesnick, R. G. Baraniuk, and N. C. Kingsbury, "The dual-tree complex wavelet transform," *Signal Processing Magazine, IEEE* **22**, 123–151 (2005).
 25. I. Daubechies, "The wavelet transform, time-frequency localization and signal analysis," *Information Theory, IEEE Transactions on* **36**, 961–1005 (1990).
 26. M. Antonini, M. Barlaud, P. Mathieu, and I. Daubechies, "Image coding using wavelet transform," *Image Processing, IEEE Transactions on* **1**, 205–220 (1992).
 27. M. N. Do and M. Vetterli, "Contourlets: a directional multiresolution image representation," in "Image Processing. 2002. Proceedings. 2002 International Conference on," , vol. 1 (IEEE, 2002), vol. 1, pp. I–357.
 28. E. J. Candes, D. L. Donoho *et al.*, *Curvelets: A surprisingly effective nonadaptive representation for objects with edges* (DTIC Document, 1999).
 29. J.-L. Starck, E. J. Candès, and D. L. Donoho, "The curvelet transform for image denoising," *Image Processing, IEEE Transactions on* **11**, 670–684 (2002).
 30. E. J. Candes and D. Donoho, *Ridgelets and their derivatives: Representation of images with edges* (Defense Technical Information Center, 2000).
 31. K. Guo and D. Labate, "Optimally sparse multidimensional representation using shearlets," *SIAM journal on mathematical analysis* **39**, 298–318 (2007).
 32. S. L. Shishkin, "Fast and robust compressive sensing method using mixed hadamard sensing matrix," *Emerging and Selected Topics in Circuits and Systems, IEEE Journal on* **2**, 353–361 (2012).
 33. C. Li, "Compressive sensing for 3d data processing tasks: applications, models and algorithms," Ph.D. thesis, Rice University (2011).
 34. C. Li, W. Yin, and Y. Zhang, "Users guide for tval3: Tv minimization by augmented lagrangian and alternating direction algorithms," (2009).
 35. E. J. Candès and M. B. Wakin, "An introduction to compressive sampling," *Signal Processing Magazine, IEEE* **25**, 21–30 (2008).
 36. R. K. Yarlagadda and R. R. Yarlagadda, *Hadamard matrix analysis and synthesis* (Kluwer Academic Publishers Boston, 1997).
 37. C. A. Metzler, A. Maleki, and R. G. Baraniuk, "From denoising to compressed sensing," *CoRR* **abs/1406.4175** (2014).
-

1. Introduction

Correlation measurements are often necessary to characterize joint systems. Unfortunately, high dimensional characterizations may not be possible due to impracticalities such as measurement time, computer memory, or even computing power. These problems arise because the problem complexity scales quadratically with the two-particle subsystem dimensionality.

One such example is the characterization of continuous-variable quantum entanglement – a resource gaining ground as an applicable tool in quantum technologies [1, 2, 3, 4, 5, 6]. An easy source of continuous variable entanglement is Spontaneous Parametric Down-Conversion (SPDC) in a nonlinear crystal [7]. Depending on the configuration, the resulting bi-photon state may be entangled in the continuous degrees of position and momentum [8, 9, 10]. To determine if the system is entangled, both the bi-photon joint-position and joint-momentum probability distributions composed of a signal and idler photon must be measured through correlation measurements.

Much work has been done recently to characterize high-dimensional position-momentum entanglement with discrete measurements [8, 11, 12, 13, 14]. Characterizations of position and momentum resulting from SPDC are done by first measuring each signal and idler in either an image plane of the crystal (constituting a position measurement) or a Fourier-transform plane of the crystal (constituting a momentum measurement) and then correlating signal and idler pixels through coincidence counting.

High-dimensional measurements of joint-systems composed of multiple particles involve many single-particle measurements. For a bi-photon probability distribution, single-particle measurements are typically done by raster scanning the individual signal- and idler-photon probability distributions. Imaging these distributions with a camera has been shown in [15, 16], yet cameras often introduce far more noise from dark-counts than a single-photon detector. However, the time-frame to complete a raster scan with a single-photon detector quickly becomes impractical and may require several months to complete certain scans.

Compressive Sensing (CS) techniques can be used instead of raster scanning and often reduce these data acquisition times from months to hours [17]. While the data-acquisition time is drastically reduced, it comes at the cost of computational complexity, requiring a computational reconstruction of the signal. The reconstruction process often becomes impossible if computing power or memory is insufficient. In this article we propose the use of fast-Hadamard transforms for high-dimensional joint-space reconstructions. We show how to implement this method to eliminate computer-memory overhead and reduce reconstruction times.

To demonstrate the effectiveness of this method, a 16.8 million-dimensional bi-photon probability distribution that would normally require well over a year to raster scan is measured in approximately twenty hours. The memory overhead of 2 terabytes (TB) in computer memory is eliminated, instead requiring between 8 and 32 gigabytes (GB), and a full reconstruction is accomplished in approximately twenty minutes.

2. Background & Motivation

A correlation measurement for SPDC consists of measuring the joint-intensities between signal and idler beams in individual signal and idler transverse planes [15, 18, 17]. These signal and idler planes constitute discrete spaces when discretized into pixels. Correlation measurements of bi-photon probability distributions are often performed by raster scanning in these spaces. To verify if the system is entangled, measurements in position and in momentum are taken by raster scanning in image and in Fourier planes of the crystal respectively. This is often accomplished with a spatial light modulator (SLM), which discretizes these planes according to the SLM's pixel resolution. To perform a simple correlation measurement between signal (S) and idler (I) systems, a pixel in one plane of system S must be correlated with every pixel within the plane

of system I .

Letting the joint-space be defined as the joint-particle probability distribution, a subspace is then defined as the individual signal and idler marginal probability distributions in their respective planes from the crystal. The joint-space correlation measurement can be described by a single operator \hat{A} that measures the bi-photon state Ψ . However, measurements on each particle are performed separately, so the joint-space measurement operator is actually composed of the tensor product of the signal and idler measurement processes $(\hat{A}_S \otimes \hat{A}_I) \cdot \Psi$. Because of this tensor-product relationship, the discrete joint-particle measurement process $\mathbf{A} \cdot \Psi$ is then the Kronecker product of the single-particle measurements $(\mathbf{A}_S \otimes \mathbf{A}_I) \cdot \Psi$. If the signal and idler spaces are each discretized into N pixels, the corresponding joint-space is composed of N^2 pixels. The required number of measurements scales quadratically with the signal and idler dimensions, therefore achieving reasonable subspace resolution scans of even $N = 16 \times 16$ becomes impractical.

CS techniques help to overcome the limitations of raster scanning by actively compressing the necessary correlated information into $M \ll N^2$ measurements by leveraging the assumption of signal sparsity [19]. CS requires that a measurement matrix subsample the signal by taking M linear projections of the signal with random patterns instead of raster scanning. The signal is then computationally reconstructed.

CS techniques were first applied to characterize entangled systems in [17] whereby measurements that would have taken the better part of a year instead only took about eight hours. Howland's paper along with this work uses a variant of the Rice single-pixel camera [20], effectively making it a double-pixel camera. Compressed sensing has also been applied to constructing the density matrix of a two-photon state in [21]. We propose a practical extension to these methods that enables a drastic increase in the measurement dimensionality while reducing reconstruction time by utilizing properties of Hadamard matrices. Performing CS on high-dimensional signals is not an entirely new problem, and several clever solutions exist. For example, utilizing separable compressive sensing matrices combined by a Kronecker product, where one sensing matrix sampled in \hat{x} and the other sensing matrix sampled in \hat{y} , enabled two-dimensional megapixel image reconstructions in [22]. Kronecker-product-based sensing matrices have also enabled CS of multidimensional signals such as those used in hyperspectral imaging. One such method known as Kronecker compressive sensing in [23] uses the Kronecker product matrices as a sparsifying basis for reconstruction. In each of these methods, the signal \mathbf{x} is sampled by a measurement matrix \mathbf{A} to produce a measurement vector $\mathbf{y} = \mathbf{A} \cdot \mathbf{x}$. Many reconstruction algorithms only require the operations $\mathbf{A} \cdot \mathbf{x}$ and $\mathbf{A}^T \cdot \mathbf{y}$ where \mathbf{A}^T is the transpose of \mathbf{A} . For extremely high dimensions, these operations become time-intensive and potentially impossible if \mathbf{A} cannot be stored in computer memory. The methods previously mentioned utilize Kronecker products to prevent storing a massive sensing matrix. However, they still require the storage of the subspace sensing matrices in computer memory, matrix-vector operations, and some even require that the sparse-basis also be separable (as opposed to current state-of-the-art overcomplete bases including wavelets [24, 24, 25, 26], contourlets [27], curvelets [28, 29], ridgelets [30], and shearlets [31]). The method outlined in this article also requires the use of Kronecker products. However, this method eliminates the storage of sampling matrices in computer memory, does not require an orthogonal sparse basis transform, and exploits the speed of fast-Hadamard transforms in reconstruction as explained in [32]. Using the randomization techniques outlined in [33] and [34], sensing matrices composed of randomized Hadamard matrices offer tremendous speed enhancements in many reconstruction algorithms.

3. Compressive Sensing

CS helps to overcome unreasonable data-acquisition times associated with sampling high-dimensional signals with limited resources. CS requires that the signal of interest $\tilde{\mathbf{x}}$ has a sparse representation \mathbf{x} via a basis transform. Limiting the discussion to real signals for simplicity, this means that if $\tilde{\mathbf{x}} \in \mathbb{R}^N$, then there exists a basis transform Ψ in which $k < N$ components of $\mathbf{x} = \Psi \cdot \tilde{\mathbf{x}}$ are nonzero; \mathbf{x} is a k -sparse representation of $\tilde{\mathbf{x}}$. CS posits that if \mathbf{x} is approximately k -sparse, then only $M > O(k \log(N/k))$ projections of $\tilde{\mathbf{x}}$ are needed to accurately sample $\tilde{\mathbf{x}}$. A typical CS technique involves taking $M < N$ projections of a signal $\tilde{\mathbf{x}}$ with a random sensing matrix $\mathbf{A} \in \mathbb{R}^{M \times N}$ to form a measurement vector $\mathbf{y} = \mathbf{A} \cdot \tilde{\mathbf{x}}$ where $\mathbf{y} \in \mathbb{R}^M$. Assuming the signal representation \mathbf{x} is k -sparse, \mathbf{x} may be recovered by solving

$$\min_{\mathbf{x}} \tau g(\mathbf{x}) \text{ subject to } \|\mathbf{y} - \mathbf{A} \cdot (\Psi^{-1} \cdot \mathbf{x})\|_2^2 < \varepsilon \quad (1)$$

where the second term is a least-squares term bounded by a predefined error ε and

$$\|\mathbf{x}\|_p := \left(\sum_{i=1}^n |x_i|^p \right)^{1/p}$$

is defined as the l_p -norm. The function $g(\mathbf{x})$ is a function to be minimized depending on the assumed sparsity; $g(\mathbf{x})$ is often chosen to be the l_1 -norm $\|\mathbf{x}\|_1$, the total variation as defined by the gradient $\|\nabla \mathbf{x}\|_1$, or a combination of functions where \mathbf{x} is known to be sparse. τ is simply a weighting term that weights the sparsity, favoring either the least-squares solution or the sparsity. Because $\mathbf{A} \in \mathbb{R}^{M \times N}$ where $M \ll N$, there are an infinite number of solutions confined to the least-squares term. The function $g(\mathbf{x})$ picks out the sparsest of these solutions. An overview of compressive sensing and its applications may be found in [35].

4. Experimental Setup for a Joint-System Measurement

The method presented in this article applies CS to a two-particle system. An experimental system for measuring the joint-space bi-photon probability distribution is presented in Figure 1. The bi-photon is composed of correlated photons, and we wish to measure the correlations between every pixel in the signal-space with every pixel in the idler-space to construct a joint-space distribution \mathbf{x}_{SI} . Figure 1 presents each particle's space as two-dimensional. Yet, to simplify the CS formalism, we represent each subspace as discretized into \mathbb{R}^N and the joint-space as a vector $\mathbf{x}_{SI} \in \mathbb{R}^{N^2}$. The bi-photon probability distribution is already k -sparse in the pixel basis due to the tight pixel correlations. This eliminates the need to define a sparse-basis such that Ψ becomes the identity operator $\Psi = \mathbb{1}$ and a measurement is represented as $\mathbf{y}_{SI} = \mathbf{A} \cdot \mathbf{x}_{SI}$ in the formalism above.

As outlined in [17], compressive sensing is experimentally accomplished by taking random projections with patterns composed of $\lceil \sqrt{N} \times \sqrt{N} \rceil$ pixels within each subspace of the signal and idler systems. A projection is acquired by placing square patterns on signal and idler SLM's and then measuring the coincidence counts after sending the light from each SLM to separate detectors.

The set of patterns for each signal and idler is represented by subspace sensing matrices \mathbf{P}_S and \mathbf{P}_I . These subspace sensing matrices are built by first reshaping each square pattern into a $[1 \times N]$ row and then stacking M different patterns into matrices to form \mathbf{P}_S and $\mathbf{P}_I \in \mathbb{R}^{M \times N}$ sensing matrices for the signal and idler subspaces respectively. These patterns are then combined using a row-wise Kronecker product to form the joint-space sensing matrix $\mathbf{A} \in$

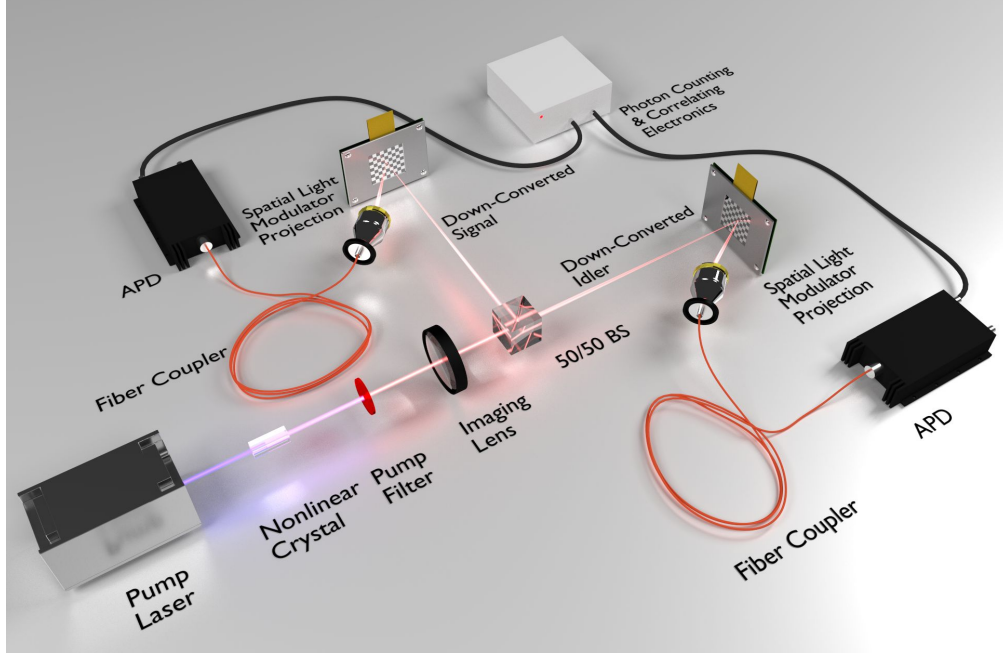


Fig. 1. The above experimental diagram demonstrates how to image a joint two-particle system. In this paper, the joint-system is composed of highly-correlated signal and idler photons from a SPDC source. The experiment samples the position distribution of the joint-system by taking random projections of signal and idler intensities with a spatial light modulator within an image plane of the crystal. An avalanche photodiode (APD) detects photon arrivals while the photon counters measure photon coincidences.

$\mathbb{R}^{M \times N^2}$ as follows:

$$\mathbf{A} = \mathbf{P}_S[i] \otimes \mathbf{P}_I[i] = \begin{bmatrix} \mathbf{P}_S[1] \otimes \mathbf{P}_I[1] \\ \mathbf{P}_S[2] \otimes \mathbf{P}_I[2] \\ \vdots \\ \mathbf{P}_S[M] \otimes \mathbf{P}_I[M] \end{bmatrix} \quad (2)$$

for $i \in 1 \dots M$ where $\mathbf{P}[i]$ represents the i^{th} row of \mathbf{P} . Because the resolution of the joint-space increases as N^2 , both the necessary computer memory to store \mathbf{A} and the reconstruction time needed to perform matrix operations quickly become formidable problems. The following sections demonstrate how Hadamard matrices are used to overcome both of the limitations of computer memory and reconstruction time when a joint-space reconstruction would normally be considered impossible.

5. Randomly Sampled & Permuted Hadamard Sensing Matrices

Hadamard matrices have a structure that is particularly advantageous to the CS framework. Hadamard matrices result from a simple construction of the following matrices:

$$\begin{aligned} \mathbf{H}_1 &= [1] \\ \mathbf{H}_2 &= \begin{bmatrix} 1 & 1 \\ 1 & -1 \end{bmatrix}. \end{aligned}$$

From these, any Hadamard-ordered matrix can be decomposed as follows

$$\mathbf{H}_{2^k} = \begin{bmatrix} \mathbf{H}_{2^{k-1}} & \mathbf{H}_{2^{k-1}} \\ \mathbf{H}_{2^{k-1}} & -\mathbf{H}_{2^{k-1}} \end{bmatrix} \quad (3)$$

using the Kronecker product

$$\mathbf{H}_{2^k} = \mathbf{H}_2 \otimes \mathbf{H}_{2^{k-1}} \quad (4)$$

for $k > 1$. Because of this structure, Hadamard matrices can be used to build patterns and a sensing matrix that utilizes the speed and efficiency of a fast-Hadamard transform $\mathcal{H}[\dots]$. We use a normally-ordered fast-transform in this work. Its algorithm is similar to that of a fast-Fourier transform, but it consists of only additions and subtractions. Hence, it is well suited to avoiding the computer memory problem of explicitly storing a sensing matrix \mathbf{A} and performs the reconstruction operations $\mathbf{y} = \mathbf{A} \cdot \mathbf{x}$ and $\mathbf{x}' = \mathbf{A}^T \cdot \mathbf{y}$ in $O(N^2 \log N^2)$ time - significantly faster than a matrix multiplication of $O(N^4)$ time. Here, $\mathbf{y} \in \mathbb{R}^M$ represents the M random projections of \mathbf{x} , and \mathbf{x}' is an approximate solution to \mathbf{x} using the transpose of \mathbf{A} . A thorough overview of Hadamard matrices, fast-Hadamard transforms, and their applications to signal and image processing may be found in [36].

To construct \mathbf{P}_S , \mathbf{P}_I , and \mathbf{A} from Hadamard matrices, the Hadamard matrices must be truncated. While Hadamard matrices are square, \mathbf{P}_S and $\mathbf{P}_I \in \mathbb{R}^{M \times N}$ while $\mathbf{A} \in \mathbb{R}^{M \times N^2}$ where $M \neq N \neq N^2$. Each matrix may be formed by taking specific rows from a Hadamard matrix with the correct dimensions. \mathbf{A} is constructed from \mathbf{H}_{N^2} while \mathbf{P}_S and \mathbf{P}_I are constructed from \mathbf{H}_N . Because of the relation in equation (2), the rows of \mathbf{A} will be determined by the rows of \mathbf{P}_S and \mathbf{P}_I . N^2 must also be a power of 2.

To build a suitable set of sensing patterns for \mathbf{P}_S and \mathbf{P}_I , the Hadamard matrices must be randomized in both their rows and columns. The sensing matrices must be both incoherent with the image yet span the space in which the signal resides. In other words, the sensing matrices must adequately sample the basis components of the signal. Random sensing matrices perform this task well. Hadamard matrices are square and naturally contain much structure. The randomization of \mathbf{H} is accomplished by randomly selecting rows of \mathbf{H} to form the patterns while randomly permuting the columns. This helps to ensure that each sensing matrix is random in appearance.

To begin constructing patterns, M rows are randomly chosen from $\mathbf{H}_N \in \mathbb{R}^{N \times N}$ to form sets of patterns for \mathbf{P}_S and $\mathbf{P}_I \in \mathbb{R}^{M \times N}$. Random rows of \mathbf{H}_N are selected by defining two vectors \mathbf{r}_S and $\mathbf{r}_I \in \mathbb{R}^M$ for each signal and idler system to be composed of M randomly chosen integers on the interval $[2, N]$. The values in \mathbf{r} state which rows should be extracted from \mathbf{H}_N . Note that the interval begins at 2 because the first row of a Hadamard matrix is composed entirely of 1's and yields no practical information in the CS framework; Most algorithms do not require the total intensity of the scene. Also, please note that $\mathbf{A} \in \mathbb{R}^{M \times N^2}$ where $M \ll N^2$. This condition allows for scenarios where $\mathbf{P}_S, \mathbf{P}_I \in \mathbb{R}^{M \times N}$ such that $M > N$ in the individual subspaces, meaning rows of \mathbf{H}_N may be repeated when constructing \mathbf{P}_S and \mathbf{P}_I .

The randomization of the Hadamard columns is accomplished by defining permutation vectors \mathbf{p}_S and $\mathbf{p}_I \in \mathbb{R}^N$ that randomly permute the N columns of \mathbf{H}_N . Once \mathbf{r} and \mathbf{p} have been defined for both the signal and idler subspaces, patterns are constructed by the following equations:

$$\begin{aligned} \mathbf{P}_S &= \mathbf{H}_N[\mathbf{r}_S, \mathbf{p}_S] \\ \mathbf{P}_I &= \mathbf{H}_N[\mathbf{r}_I, \mathbf{p}_I] \end{aligned} \quad (5)$$

where the y and x components of $\mathbf{H}[y, x]$ refer to the rows and columns of \mathbf{H} respectively.

The operations of \mathbf{r} and \mathbf{p} effectively randomize the patterns \mathbf{P} in the signal and idler subspaces. Although these operations are defined for the signal and idler subspaces, they combine in a particular way according to equation (2) to construct a Hadamard-based sensing matrix \mathbf{A} that enables fast transform operations in the joint-space. The manner in which they combine to manipulate a Hadamard matrix \mathbf{H}_{N^2} that spans the joint-space is detailed in the next section.

6. Joint-Space Hadamard Sensing Matrices

Once \mathbf{P}_S and \mathbf{P}_I have been constructed from \mathbf{r} and \mathbf{p} , they must be used to construct \mathbf{A} . From equations (2) and (4), it is clear that if \mathbf{P}_S and \mathbf{P}_I are Hadamard matrices, then \mathbf{A} will be a subset of a Hadamard matrix. For example, letting \mathbf{r} and $\mathbf{p} \in \mathbb{R}^N$ be non-permuting vectors of $[1, 2, 3, \dots, N]$, then equation (2) states that the sensing matrix would simply be

$$\mathbf{A} = \begin{bmatrix} \mathbf{H}_N[1] \otimes \mathbf{H}_N[1] \\ \mathbf{H}_N[2] \otimes \mathbf{H}_N[2] \\ \vdots \\ \mathbf{H}_N[N] \otimes \mathbf{H}_N[N] \end{bmatrix}.$$

Therefore, simply knowing how \mathbf{r} and \mathbf{p} in the signal and idler subspaces combine to form their corresponding joint-space row-selection and permutation vectors, \mathbf{r}_{SI} and \mathbf{p}_{SI} , will enable the use of fast-Hadamard transforms without ever having to explicitly construct \mathbf{A} .

Consider the construction of \mathbf{r}_{SI} first. By equation (4), the complete joint-space sensing matrix \mathbf{A} is simply formed by the row-wise Kronecker product of the subspace sensing matrices \mathbf{P}_S and \mathbf{P}_I . As \mathbf{r}_S and \mathbf{r}_I determine the ordering of the Hadamard rows within these patterns, \mathbf{r}_{SI} must also be a subset of a Kronecker product of \mathbf{r}_S and \mathbf{r}_I . Knowing that the Kronecker product of \mathbf{P}_S and \mathbf{P}_I will form “blocks” of size $[M \times N]$, it is straightforward to show that

$$\mathbf{r}_{SI}[i] = N(\mathbf{r}_S[i] - 1) + \mathbf{r}_I[i] \quad (6)$$

for $i \in 1 \dots M$ where $\mathbf{r}[i]$ represents the i^{th} component of \mathbf{r} . Note that element-wise counting in this article starts at 1 and not 0.

Because \mathbf{r}_S and \mathbf{r}_I are chosen at random and will often be over-complete, $M > N$, \mathbf{r}_{SI} will probably have repeating units and a row within \mathbf{A} will appear more than once. This is equivalent to taking the same projection more than once, offering no additional information. An easy way to fix this problem is to simply compare each of the values within \mathbf{r}_{SI} and eliminate repeating i^{th} values. If $\mathbf{r}_{SI}[i]$ is a repeated value, eliminate $\mathbf{r}_{SI}[i]$ along with the components $\mathbf{r}_S[i]$ and $\mathbf{r}_I[i]$. In this way, the number of samples M will decrease yet contain the same amount of information.

The formation of \mathbf{p}_{SI} follows a similar form as \mathbf{r}_{SI} , yet it will be of length N^2 . Although it is not a simple Kronecker product, it does follow from the structure in equation (2). The structure of \mathbf{p}_{SI} takes the form

$$\mathbf{p}_{SI}[N(i-1) + j] = N(\mathbf{p}_S[i] - 1) + \mathbf{p}_I[j] \quad (7)$$

for $i \in 1 \dots N$ and $j \in 1 \dots N$. Generating randomized Hadamard matrices using \mathbf{r} and \mathbf{p} for each signal, idler, and joint-space are summarized below:

$$\begin{aligned} \mathbf{P}_S &= \mathbf{H}_N[\mathbf{r}_S, \mathbf{p}_S] \\ &= \mathbf{H}_N[\mathbf{r}_I, \mathbf{p}_I] \\ \mathbf{H}_{N^2}[\mathbf{r}_{SI}, \mathbf{p}_{SI}] \end{aligned} \quad (8)$$

where, again, the y and x components of $\mathbf{H}[y, x]$ refer to the rows and columns of \mathbf{H} respectively. While each pattern associated with a specific row of \mathbf{P}_S and \mathbf{P}_I needs to be formed and

reshaped into $[\sqrt{N} \times \sqrt{N}]$ arrays to take projections in the signal and idler subspaces using SLM's, \mathbf{A} never needs to be generated or stored in memory for reconstruction. Even generating the lower dimensional subspace matrices in entirety can be cumbersome if computer memory is insufficient. The following section demonstrates how to construct individual patterns of \mathbf{P}_S and \mathbf{P}_I to sample \mathbf{x}_{SI} without ever having to formally build the matrices that represent the set of all patterns for \mathbf{P}_S , \mathbf{P}_I , or \mathbf{A} using only \mathbf{r} and \mathbf{p} .

7. Fast Hadamard Transforms Utilizing \mathbf{r} & \mathbf{p}

Keeping track of the randomization operations applied to \mathbf{P}_S , \mathbf{P}_I , and \mathbf{A} allow the use of fast-Hadamard transforms. Equations (6) through (8) demonstrate that each pattern and sensing matrix is dependent upon the four vectors: \mathbf{r}_S , \mathbf{r}_I , \mathbf{p}_S , and \mathbf{p}_I . Coupling this knowledge with a fast-Hadamard transform alleviates the need to ever store \mathbf{P}_S , \mathbf{P}_I , or \mathbf{A} in computer memory. This is done by reordering either \mathbf{x} or \mathbf{y} to be fast-Hadamard transformed according to \mathbf{p} and then picking specific elements from the final result according to \mathbf{r} . The manner in which they are rearranged and picked depends upon the operation $\mathbf{A} \cdot \mathbf{x}$ or $\mathbf{A}^T \cdot \mathbf{y}$ in either the data acquisition or reconstruction processes.

Starting with the data-taking procedure $\mathbf{y} = \mathbf{A} \cdot \mathbf{x}$, projections are taken of each signal and idler system. The data-taking operation requires a true matrix multiplication according to the experiment where the joint two-particle distribution is multiplied by a Kronecker product of the SLM patterns before reaching detectors. When using fast-Hadamard transforms, any individual pattern in \mathbf{P}_S , \mathbf{P}_I , or \mathbf{A} may be retrieved without having to store them first in memory. Pattern construction is done by fast-Hadamard transforming basis vectors and then permuting them. Because of the symmetric nature of a Hadamard matrix, a fast-Hadamard transform of a basis vector $\alpha[i]$, in which the i^{th} component is equal to one and the rest zeros, is equal to the i^{th} row of the Hadamard matrix $\mathbf{H}[i]$. In short, $\mathcal{H}[\alpha[i]] = \mathbf{H}[i]$. Hence, every i^{th} pattern $\mathbf{P}[i, \dots]$ can be built according to a fast transform by

$$\begin{aligned} \mathbf{H}[i, \dots] &= \mathcal{H}[\alpha[\mathbf{r}[i]]] \\ \mathbf{P}[i] &= \mathbf{H}[i, \mathbf{p}] \end{aligned} \quad (9)$$

for $i \in 1 \dots M$ where $\alpha[\mathbf{r}[i]]$, a basis vector whose $\mathbf{r}[i]^{th}$ component is equal to 1, is fast-Hadamard transformed and then permuted according to \mathbf{p} .

To take experimental data, many SLM's, such as digital micromirror devices, are operated in a binary fashion of on or off - transmitting light either to or away from a detector. If only using one detector per subspace, at any given moment a pattern may only be composed of 0's or 1's while Hadamard matrices are composed of 1's and -1's. To display the full Hadamard pattern with one detector per subspace, the data-taking operations must be split into positive and negative operations. \mathbf{H}_{N^2} may be decomposed into a sum of four Kronecker products of both positive \mathbf{H}_N , represented by \mathbf{H}_N^+ which is composed of 0's and 1's, and negative \mathbf{H}_N , represented by \mathbf{H}_N^- which is composed of -1's and 0's.

$$\mathbf{H}_{N^2} = \mathbf{H}_N^+ \otimes \mathbf{H}_N^+ + \mathbf{H}_N^- \otimes \mathbf{H}_N^- + \mathbf{H}_N^+ \otimes \mathbf{H}_N^- + \mathbf{H}_N^- \otimes \mathbf{H}_N^+. \quad (10)$$

This means that a single projection $\mathbf{y}[i] = \mathbf{A}[i] \cdot \mathbf{x}$ will require four coincidence measurements of the correlations between the two subsystems per y-vector component. Even though $4M$ coincidence measurements are required when using one detector per subspace, the drastic sampling performance gained through CS methods is such that $4M \ll N^2$. Alternatively, if two detectors are used in each subspace (one detector to collect positive components and one detector to collect the negative components), the detection process could be streamlined to measure each of the four correlations in equation (10).

In reconstruction, fast-Hadamard transforms may be utilized by CS reconstruction algorithms to perform forward and inverse operations. The operation $\mathbf{A} \cdot \mathbf{x}$ is done entirely via fast-Hadamard transform. However, as no permuted matrix will be used in multiplication, \mathbf{x} must instead be inverse-permuted before being fast-transformed. The inverse-permutation is done by defining an inverse permutation vector \mathbf{q} as

$$\mathbf{q}[\mathbf{p}[i]] = i \quad (11)$$

for all i elements in \mathbf{p} . The forward operation $\mathbf{A} \cdot \mathbf{x}$ requires that \mathbf{x} first be inverse-permuted, fast-transformed, and then finally have the correct M elements extracted from the final result. This is accomplished with the following operations

$$\begin{aligned} \mathbf{y}' &= \mathcal{H}[\mathbf{x}[\mathbf{q}_{SI}]] \\ \mathbf{y} &= \mathbf{y}'[\mathbf{r}_{SI}]. \end{aligned} \quad (12)$$

The inverse operation $\mathbf{A}^T \cdot \mathbf{y}$ requires that a vector β composed of N^2 zeros be filled with the elements of \mathbf{y} according to \mathbf{r}_{SI} , fast-transformed, and then permuted according to \mathbf{q} as follows:

$$\begin{aligned} \beta[\mathbf{r}_{SI}] &= \mathbf{y} \\ \mathbf{x}[\mathbf{q}_{SI}] &= \mathcal{H}[\beta]. \end{aligned} \quad (13)$$

These operations work because Hadamard matrices are symmetric $\mathbf{H} = \mathbf{H}^T$. Because of this structure, the operations $\mathbf{A} \cdot \mathbf{x}$ and $\mathbf{A}^T \cdot \mathbf{y}$ can be utilized by most reconstruction algorithms and operate much faster without matrix-vector multiplications or ever having to store \mathbf{A} in memory.

The methods outlined in this article can also be applied to signals that are not sparse in the “pixel-basis” where $\Psi \neq \mathbb{1}$. Sparse forward and inverse transform operations, $\Psi[\dots]$ and $\Psi[\dots]^{-1}$, need to be applied to \mathbf{x} in an appropriate order to bring \mathbf{x} and \mathbf{y} back into the pixel-basis before fast-Hadamard transforming. The forward operation requires that a sparse inverse transform be applied before implementing our Hadamard method, $\mathbf{A} \cdot \Psi[\mathbf{x}]^{-1}$, while the reverse operation requires that a forward sparse transform be applied after implementing our Hadamard method, $\Psi[\mathbf{A}^T \cdot \mathbf{y}]$. While the complexity certainly increases, the memory overhead is still minimal, especially if a fast and in-place sparse transform $\Psi[\dots]$ is known.

To summarize, the algorithms for calculating $\mathbf{A} \cdot \Psi[\mathbf{x}]^{-1}$ and $\Psi[\mathbf{A}^T \cdot \mathbf{y}]$ are listed below.

- $\mathbf{y} = \mathbf{A} \cdot \Psi[\mathbf{x}]^{-1}$
 1. If $\Psi = \mathbb{1}$, neglect this step. Otherwise, inverse transform \mathbf{x} out of the sparse basis using the inverse transform to obtain $\mathbf{x}' = \Psi[\mathbf{x}]^{-1}$.
 2. Inverse permute \mathbf{x}' using \mathbf{q}_{SI} such that $\mathbf{x}'' = \mathbf{x}'[\mathbf{q}_{SI}]$.
 3. Fast-Hadamard transform \mathbf{x}'' such that $\mathbf{y}' = \mathcal{H}[\mathbf{x}'']$.
 4. Extract M elements from \mathbf{y}' using \mathbf{r}_{SI} to obtain $\mathbf{y} = \mathbf{y}'[\mathbf{r}_{SI}]$.
- $\mathbf{x} = \Psi[\mathbf{A}^T \cdot \mathbf{y}]$
 1. Construct a null-vector $\beta \in \mathbb{R}^{N^2}$.
 2. Place the components of \mathbf{y} into β using \mathbf{r}_{SI} to assign the locations for the elements of \mathbf{y} such that $\beta[\mathbf{r}_{SI}] = \mathbf{y}$.
 3. Fast-Hadamard transform β such that $\beta' = \mathcal{H}[\beta]$.
 4. Permute the elements of β' using \mathbf{p}_{SI} to obtain $\mathbf{x}' = \beta'[\mathbf{p}_{SI}]$.

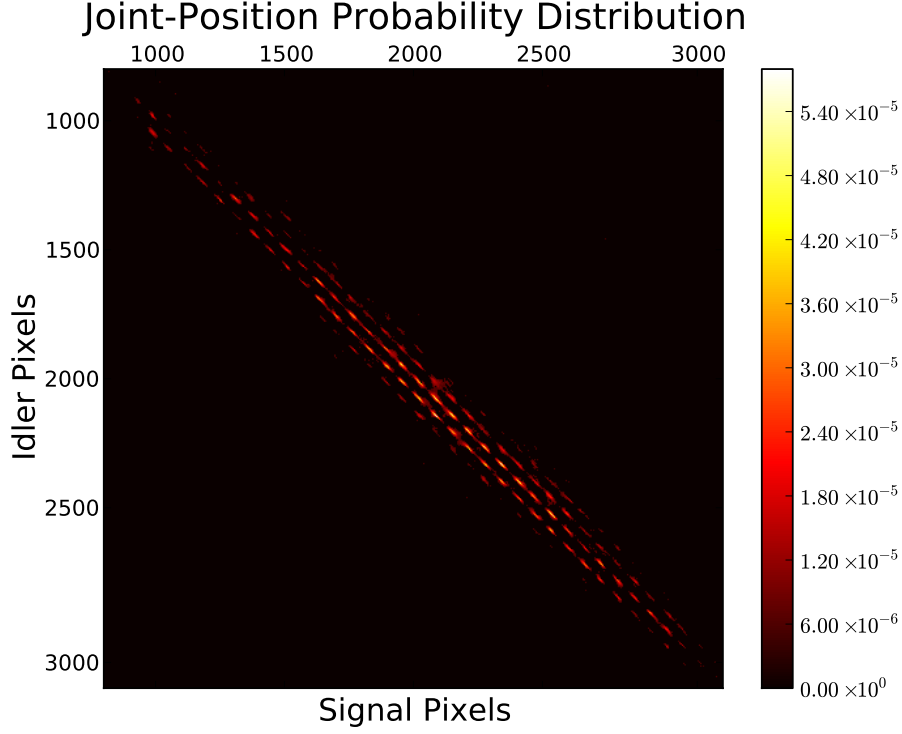


Fig. 2. This figure depicts the 64^4 (16.8×10^6) dimensional reconstructed bi-photon probability distribution in position from SPDC. This data was attained compressively with $M = 16,368$ ($.00098 \times 64^4$) samples in approximately twenty hours and was reconstructed in approximately twenty minutes. The figure above enlarges this region of the distribution because all other pixels have approximately zero probability.

5. If $\Psi = \mathbb{I}$, neglect this step and let $\mathbf{x} = \mathbf{x}'$. Otherwise, transform \mathbf{x}' into the sparse basis to obtain $\mathbf{x} = \Psi[\mathbf{x}']$.

Note the simplicity in this method. A user only needs to construct \mathbf{r} , \mathbf{p} , and \mathbf{q} for the signal, idler, and joint-space systems. These are simple calculations to perform using equations (6),(7),and (11). It also permits the use of most CS reconstruction algorithms. Because of the simplicity and freedom associated with this method, we believe it will provide a useful tool for high-dimensional joint-space reconstructions as demonstrated in the next section.

8. Compressive Measurement of a 64^4 -Dimensional Bi-photon Probability Distribution

In an experimental realization of the above algorithms, the nature of high-dimensional CS may be appreciated when measuring the joint-space of a bi-photon state from SPDC. This work is closely related to the work performed in [17], although at much higher dimensions. In this experiment, a pump laser of 405 nm drives the SPDC process in a nonlinear bismuth-borate crystal, and correlations within the image plane of the crystal are measured. A typical raster scan of the joint-space requires that each pixel in the signal domain be compared with a full raster scan of the idler domain. This requires exactly 64^4 (16.8×10^6) measurements. Assuming

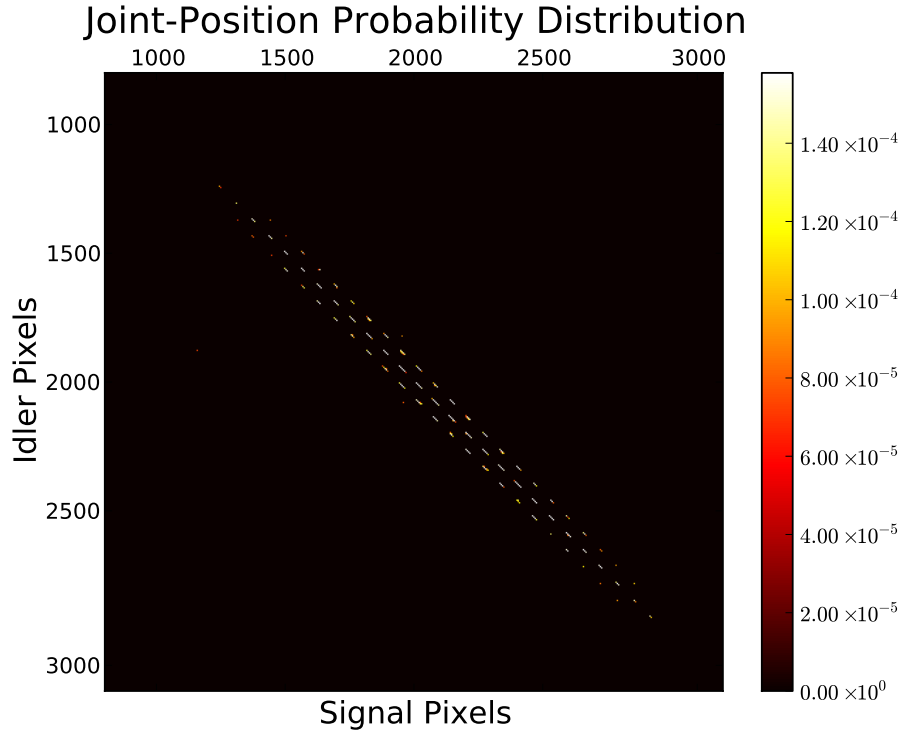


Fig. 3. This figure depicts a simulated CS reconstruction of a 64^4 (16.8×10^6) dimensional bi-photon probability distribution in position from SPDC. The simulation was done compressively with $M = 16,368$ ($.00098 \times 64^4$) under noiseless condition in approximately five minutes on a laptop with 8 GB of RAM. The figure above enlarges this region of the distribution because all other pixels have approximately zero probability. This simulation was made to serve as reference for comparison. Even though the data in Figure 2 is noisy and slightly magnified, it is in excellent agreement.

a very optimistic two-second integration time per projection, this measurement would require over a year to complete.

Compressive sensing proves to be an invaluable tool by requiring only a small fraction of the necessary measurements to accomplish the same task. Knowing that the signal is extremely sparse due to the tight correlations between the two photons, only 16,368 ($\approx .098\%$ of 64^4) measurements were necessary to accurately measure the joint-space. The number of measurements used was arbitrarily chosen as a reasonable balance between reconstruction quality and overall integration time. After deciding on a four-second integration time per projection, this is approximately a twenty-hour scan. However, the necessary sensing matrix to reconstruct the joint-space requires approximately 2.74×10^{11} elements. If operating in double-precision where each element is 8 bytes, 2 TB of RAM are required to store the sensing matrix. In contrast, a computer operating with only 8GB of RAM and an Intel-i5 mobile processor is sufficient to perform an adequate reconstruction in approximately five minutes after five iterations of an approximate message passing algorithm with a Gaussian denoiser D-AMP [37].

Unfortunately, while the results returned by the Gaussian denoiser are legible, they contain

much noise. To handle the significant presence of noise, a Bayesian least squares denoiser was used to return Figure 2. The denoising operation was demanding on computer memory and required 32 GB of RAM to perform two iterations in about twenty minutes without caching to the hard-drive. Figure 3 represents a computer simulation measuring the bi-photon position distribution with CS under noiseless conditions using less than 8 GB of RAM. Figure 2 shows the experimental final reconstruction of a 64^4 dimensional joint-space bi-photon position distribution after two iterations of D-AMP. The two figures are in excellent agreement.

9. Conclusion

This article describes in detail the methods necessary to perform high-dimensional compressive Kronecker imaging of a joint-system. By randomizing Hadamard matrices and utilizing fast-Hadamard transforms, CS is performed in the 16.8 million-dimensional Kronecker space of a bi-photon probability distribution. The experiment that would have required over a year to raster scan is performed in twenty hours. 2 TB of memory overhead associated with storing a sensing matrix is eliminated, and a full reconstruction is performed in approximately twenty minutes. We believe these methods will prove to be an invaluable tool in measuring the distribution functions of correlated systems as well as other correlation-based CS implementations.

10. Acknowledgements

We would like to thank Gregory A. Howland for the use of his computer code to verify our results and James Schneeloch for the useful discussions and advice to make this a coherent article. This work was sponsored by the Air Force grant AFOSR Grant No. FA9550-13-1-0019.